Categorizing the Meteorological Origins of Critical Ramp Events in Collective Photovoltaic Array Output

SONYA J. WELLBY

Fenner School of Environment and Society, Australian National University, Canberra, Australian Capital Territory, Australia

NICHOLAS A. ENGERER

National Information and Communications Technology Australia, Canberra, Australian Capital Territory, Australia

(Manuscript received 19 April 2015, in final form 1 November 2015)

ABSTRACT

Photovoltaic (PV) solar power use is increasing globally. The Australian Capital Territory (ACT) has legislated a renewable energy target of 90% by 2020; to reach this target, use of distributed PV solar arrays is expected to increase. Cloud cover can cause the power output of PV installations to rapidly increase or decrease, resulting in ACT-wide collective ramp events. Accurate forecasts of when the ramp events will occur are needed for electricity providers to plan for these abrupt output changes and to ensure that electricity supplies remain stable. This paper categorizes the weather events that cause changes in the output of rooftop PV arrays in the ACT, providing a foundation for future PV output forecasting to be based on weather event identification. This paper identifies citywide collective ramp events, which occur when a 60% change in collective PV power output (with respect to the clear-sky potential) is experienced within 60 min. Such events are termed critical collective ramp events. Throughout the period between January 2012 and July 2014, 34 critical ramp events occurred. Eighteen of these events were positive collective ramp events, caused most frequently by Australian northwest cloud bands and radiation fog dissipation. Sixteen negative collective ramp events were recorded, and they were caused most frequently by the passage of cold fronts and thunderstorms. The categories developed herein will make it possible to improve short-term solar forecasting methods and to enable meteorologists to contribute to forecasting critical events.

1. Introduction

Global use of renewable energies, such as solar power, is increasing. In the decade ending in 2012, solar photovoltaic (PV) generation expanded by 50% worldwide. By the end of 2012, solar PV produced almost 100 TWh of energy globally (IEA 2013). This trend is similarly observed in Australia. In 2013, household-scale solar energy generation contributed 1.62% of total Australian energy generation and produced 10.9% of the nation's renewable electricity. Nearly all of this growth has come from the accelerated uptake of rooftop PV arrays, which increased in number from 2629 to over 1.2 million between 2007 and 2013 (CEC 2013). This is a long-term trend; solar energy is expected to compose between 11% and 30% of Australia's national generation capacity, and 3%–7% of electricity generation, by 2022 (SunWiz 2012).

Solar PV power generation is primarily dependent on cloud cover. In the absence of clouds, power production follows a smooth, predictable diurnal curve as the sun moves across the sky. This is known as the PV system's clear-sky curve (Engerer and Mills 2014). The presence of clouds, however, will disrupt this relationship, resulting in reduced or, in some cases, increased power output [see the discussion of "cloud enhancement" in Zehner et al. (2010) and Engerer (2015)] relative to the clear-sky case. The relationship between electricity generation and cloud cover has consequences for both the quantity and quality of the electricity generated by a given PV system. This is best illustrated with the following examples. First, consider the impact of scattered fair-weather cumulus clouds. These may temporarily reduce power output on the scale of seconds to minutes before skies clear again. From the perspective of the

Corresponding author address: Nicholas A. Engerer, Fenner School of Environment and Society, Australian National University, Building 141, Linnaeus Way, Canberra, ACT 2601, Australia.
E-mail: nicholas.engerer@anu.edu.au

DOI: 10.1175/JAMC-D-15-0107.1

electricity sector, these clouds have a negative influence on power quality (as the power generation is unreliable and variable), but only minimally affect power quantity, as overall conditions are clear and power output is at a maximum during most time periods. Another well-suited example is an opaque stratus cloud deck, which reduces power output over the course of several hours (Engerer 2011). In this situation, power quantity is greatly reduced, but power quality only decreases minimally as power generation is fairly stable. From the perspective of an atmospheric scientist, a clear relationship should be readily apparent between the prevailing meteorological conditions and the power output of a given PV system; this is a preliminary example of how meteorologists' understanding of such concepts will prove invaluable in the development of weather-based PV forecasts (as discussed in section 1b).

As solar PV generators are added to local electricity networks, the need for grid operators to actively respond to cloud-induced changes in PV output grows. Any significant surplus or deficit of generation from embedded PV generators must be balanced by a corresponding decrease or increase in power—produced by other generating units—or an increase or decrease in local demand, in order to maintain the supply and demand balance. Ideally, this supply and demand settlement will happen well in advance of any significant changes in PV output. An important first step in preparing for such changes—for example, by developing relevant forecast algorithms—is understanding which meteorological phenomena cause disruptions in solar PV power supply. Of particular interest are events that drive a step change in the power quantity produced by a large number of PV generators over a short period of time (additionally negatively affecting power quality), as such events are most likely to affect power output. However, full climatologies of the events that cause changes in PV systems have not yet been developed. These are necessary if forecasts of PV output are to make use of the relationship between meteorological conditions and power output (see section 1b for further discussion). While PV output forecasts have traditionally been the focus of the machine learning (ML) community, the meteorological community can bring expertise and knowledge of connections between changes in cloud cover and solar irradiance, contributing both to the development of climatologies of weather events involving sudden changes in PV output, and future forecasts of such weather events. The first step in developing such climatologies is identifying which weather types are associated with ramp events, which provides clear motivation for this paper. This study will identify and categorize the meteorological events that contribute to abrupt changes in PV output at the mesoscale and synoptic scale in the city of Canberra, Australian Capital Territory (ACT), Australia (see Fig. 1), a city with over 16 500 embedded small-scale PV systems (as of December 2014).

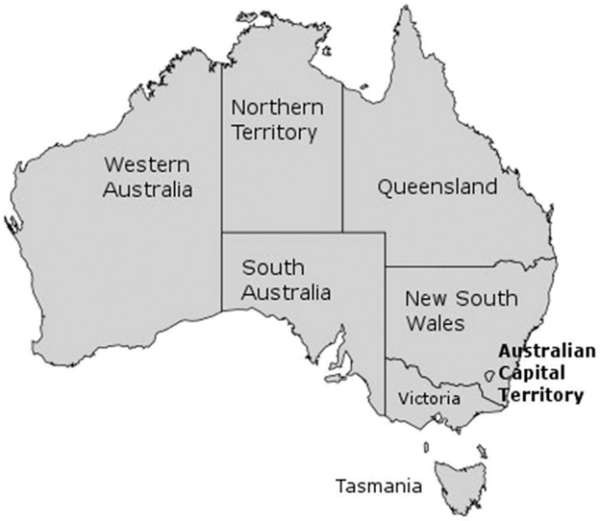

FIG. 1. Australia, with the ACT shown in boldface text. The city of Canberra is located in the northern region of the ACT.

a. *Literature review*

The relationship between changes in cloud cover and solar PV power output is well established in both observation (Jewell and Unruh 1990) and simulation studies (Engerer 2011). Solar PV arrays are sensitive to immediate changes in irradiance. This instantaneous reaction and the often abrupt nature of cloud boundaries causes the power output from solar PV to experience step change events where power production suddenly increases or decreases. These are referred to as ramp events; a sudden decrease in daytime cloud cover is termed a positive ramp event, while its opposite is termed a negative ramp event (Jewell and Unruh 1990).

The nature of ramp events changes significantly when more than one solar PV site is considered, as the diverse spatial distribution of these systems leads to complex interactions with cloud boundaries. As such, ramp events have been observed at widely varying geographic and temporal scales (Lave et al. 2012; Florita et al. 2013). This concept was first termed dispersion by Hoff and Perez (2010b), who noted that the change in output between PV sites decreases as a function of the separation distance between sites. Dispersion has been investigated by several complementary studies, each examining different scales. Murata et al. (2009) first examined dispersion at the spatial scale of hundreds of kilometers using 52 PV generators in Japan. The

magnitude of power output change is less for a group of these dispersed or ''distributed'' systems than for an individual system; the change in power output between individual systems more than 50 km apart was not correlated. With further investigation, it was discovered that geographic dispersion of PV generators tends to ''smooth'' the effects of sudden changes at a specific locality when considering generation from the entire collective of PV generators. The concepts of dispersion and smoothing were further developed at a much smaller, suburb-scale sensor network by Lave et al. (2012), who used eight radiation sites with 1″-resolution data and a maximum separation distance of 2.4 km. For their relatively dense network, they found that changes in radiation were independent at resolutions below 5′, observing clear smoothing effects. Another study (Bing et al. 2012) investigated correlations at a regional spatial scale (1775 km^2) using 71 radiation measurement stations with 10′, 5′, and 1′ data resolutions in the Sacramento Municipal Utility District in central California. Additionally, cloud speed affects site-to-site correlations: faster cloud speeds lead to higher correlations between sites separated by shorter distances (Bing et al. 2012; Hoff and Perez 2010a; Lave and Kleissl 2013).

Broad-scale ramp events, or ''collective ramp events,'' occur when all of the generators (or radiation sites) in a given region experience a similar step change in available solar radiation (Jamaly et al. 2013; Kleissl 2013). For time scales greater than 1 min, the sites affected by a collective ramp event can be as far apart as 1000 km (Murata et al. 2009). Collective ramp events are of greatest interest, as step changes affecting all generators on the scale of minutes and hours pose the greatest risk to electricity utilities (Kleissl et al. 2012). If a collective PV ramp event is experienced—that is, most PV arrays in a city simultaneously ramp up or ramp down—then the impact of distributed PV systems on grid stability is at a maximum during that period. Although electrical utilities have managed changes in load following to date, their ability to do so is diminished as PV solar systems increase their network penetration. As solar-based stability issues emerge, grid operators will then be left with two choices: halt the installation of distributed solar PV systems or forecast these changes with enough lead time to actively balance the changes with other generation systems available to the network (natural gas peakers, pumped hydro, etc.) (Maisano et al. 2016). This manuscript uses applied meteorological methods to support the second option by categorizing the weather events associated with ramp events; this will allow for the future development of event climatologies and paves the way for developing forecasts of weather types that cause ramp events, possibly through automated weather pattern detection (Wong et al. 2008) or statistical forecasting methods that operate with awareness of the prevailing weather pattern (Boland 2015).

b. *Motivation*

Accurate forecasts of the timing and magnitude of collective ramp events, provided well in advance of the events themselves, could allow grid operators to adequately prepare for their occurrence. However, to date, very few solar forecasting methods have placed special emphasis on collective ramp events, preferring instead to focus on general time series forecasting (Reikard 2009; İzgi et al. 2012; Marquez et al. 2013; Huang et al. 2013). While Jamaly et al. (2013) analyze the accuracy of collective-ramp-event forecasts estimated from satellite and weather station solar irradiance data, such information is not always readily available. Furthermore, forecasts obtained from weather station solar irradiance data—the more globally accessible of the two data sources—were least accurate. Of particular interest are the short-term forecast horizons of 0–4 h—research into which is dominated by statistical forecasting approaches, such as ML (Shi et al. 2011). Yet the approaches discussed in the literature have thus far reduced meteorological factors to simple input feature vectors, which have yielded little to no improvement in forecast accuracy (Engerer and Wellby 2014). Recently, it has been suggested that collective ramp events could be clearly connected to repeatable meteorological phenomena (Engerer and Wellby 2014), and that current methods in ML forecasting could benefit by using categories representing these weather events as input feature vectors, rather than using raw data (Engerer 2013). The regularly reported (and thus easily accessible) meteorological parameters used for ordinary weather forecasting could be used to form these categories, offering an advantage over the method of Jamaly et al. (2013).

While the literature on solar PV output forecasting recognizes the importance of cloud cover (Lorenz et al. 2009), very few studies have examined the relationship between PV output and weather events more deeply (Engerer and Wellby 2014). Several studies have noted the impact of meteorology on PV generation; for example, Nonnenmacher et al. (2014) find that fog can impact PV output readings, and Yang et al. (2014) note that solar irradiance forecast accuracy is affected by the meteorological conditions of different seasons. However, minimal research has been conducted that attempts to categorize the meteorological phenomena that cause changes in PV output. Almost all studies that attempt this restrict themselves to categorizing the basic

weather type; for example, several studies used symbolic weather categories (such as ''sunny,'' ''fair,'' and ''showers'') from numerical weather prediction (NWP) information to predict PV output (Chel and Tiwari 2011; Shi et al. 2011; Detyniecki et al. 2012). Chen et al. (2011) developed this work by predicting PV output from individual parameters that reflect changes in weather (such as relative humidity and air pressure), although no attempt was made to group the parameters according to the weather type that caused them (e.g., a midlatitude cyclone).

Almost all research involving weather categorization has so far been limited to localized, symbolic categorization (such as sunny or rainy). The exception to this is a small number of studies that link synoptic-scale marine-layer fog, stratus conditions, and frontal activity to PV production (Kleissl et al. 2012; Mathiesen et al. 2013; Jamaly et al. 2013). This paper fills this void by categorizing the mesoscale and synoptic-scale meteorological events leading to collective ramp events in Canberra. Additionally, it is hypothesized that creating categories of weather events that cause collective ramp events at a given location will allow for great improvements in the existing statistical solar forecasting routines. Fluctuations in PV output of the horizon examined in this paper are most easily forecast and, thus, are easily incorporated into forecasting algorithms (Kleissl et al. 2012). This could be accomplished, for example, by first training an ML algorithm to recognize a meteorological phenomenon (i.e., repeatable mesoscale and synoptic-scale critical-ramp-event weather types) based on the provided characteristics of the event, and then providing that preprocessed information to an ML solar forecasting model via a feature vector. This process could be applied to many regions of the globe where distributed PV systems are affected by reoccurring weather types. Once the weather events that affect a given location are known, ML algorithms can then be developed to automatically detect such events (Wong et al. 2008).

Forecasts of ramp events will require much involvement from the meteorological community. Weather-based ramp-event forecasts will rely on the development of weather-related feature vectors, which in turn require the weather events causing ramp events to be initially categorized. This provides the basis of this study's motivation to categorize the meteorological origins of ramp events for a given location. Beyond the potential benefits of improving short-term solar forecasts, the analysis in itself is novel and opens several avenues of subsequent research. Could PV systems be used to sample atmospheric radiation at much higher spatial frequencies than have previously been possible (Engerer and Xu 2015)? Could PV system power output be used in the detection and characterization of clouds? The union of these meteorological and PV power output datasets has interesting implications for the future of applied meteorology that are only now just beginning to emerge.

c. *Structure*

This paper will examine collective ramp events (hereinafter referred to as ramp events) that impact distributed PV arrays on a scale from minutes to hours. We use the term distributed PV systems to refer to those that produce electricity at or near the point of consumption (e.g., rooftop solar) and are geographically dispersed within a given region (Murata et al. 2009). The study will use from tens to hundreds of data points at the city scale (a region of approximately 25 km $\times$ 35 km) in Canberra. We have selected Canberra as the location of this study as it has legislated a renewable energy target of 20% by the year 2020; meeting this target will depend heavily on use of solar installations. Canberra has one of the most ambitious renewable energy targets in the world, and, as such, the ability of grid operators to actively manage collective ramp events in the region is a high priority. The study will focus on identifying city-scale ramp events that occur *despite* the mitigating effect of geographic smoothing; as such, the analysis is restricted to ramp events that are experienced collectively across the city. By identifying these citywide ramp events, it is possible to categorize the events according to the mesoscale and synoptic-scale meteorological phenomena that produced them. A discussion of the origin and nature of the weather patterns that caused them will be provided.

2. Data and methods

Two principal analyses were undertaken as part of this study. The first analysis involved identifying which dates in the study period were associated with ramp events. The second portion of the study consisted of identifying and analyzing the meteorological events responsible for causing the ramp events in question.

The PV data were obtained from an open Internet site (http://PVOutput.org) at which system owners voluntarily report their power output data and the characteristics of their PV array. This dataset is publicly available and as of July 2014 included over 240 sites in the Canberra municipality. The data were collected from 2 January 2012 to 17 July 2014 and aggregated to 10-min intervals using the sum of the total power output normalized to the sum of the rated installed capacity. We then identified positive and negative 60-min ramp events by calculating the ramp rate according to the method of Lave and Kleissl (2010). Equation (1) presents

the ramp-rate (RR) calculation (kW kW_p^{-1} min^{-1}), where PV_{meas} is the measured PV output (kW) and PV_{clr} is the clear-sky potential (kW_p). The required clear-sky estimate was generated by the K_{PV} methodology developed in Engerer and Mills (2014):

$$RR = \frac{PV_{meas_t} - PV_{clr_t} - (PV_{meas_{t-60}} - PV_{clr_{t-60}})}{60\,\text{min}}. \quad (1)$$

Ramp events that exceeded a critical threshold of 60% of the clear-sky potential within 60 min (equivalent to an average ramp rate of 1% min^{-1}) were identified as ''critical ramp events'' and subjected to further meteorological analysis for categorization:

$$\frac{|PV_{meas_t} - PV_{meas_{t-60}}|}{\overline{PV_{clr_{t,t-60}}}} > 0.6. \quad (2)$$

The second component of the analysis was undertaken using meteorological data sourced from the Australian Bureau of Meteorology (BoM). Data sources for the analysis included weather observations from the weather station at the Canberra Airport (BoM station 070351; WMO identifier 94926), NWP output from the BoM Australian Community Climate and Earth-System Simulator (ACCESS) model, archived mean sea level pressure (MSLP) charts, and satellite imagery provided by the Japanese Meteorological Agency's Geostationary Meteorological Satellite system. These data sources were used to manually identify which weather events were associated with each ramp event.

Information regarding the PV dataset

Note that the number of PV sites used to obtain output data increased over the course of the analysis (see Fig. 2); the median number of sites used to analyze a ramp event was approximately 92, the minimum number was 21 sites, and the maximum number of sites was 240. For each ramp event presented, the number of PV sites reporting data at the given time is included (number of stations $n = x$). The increase in sites was due to growth in the number of users actively reporting data to the PVOutput server. We recognize that it is possible that this could result in falsely identifying broad-scale ramp events during periods when relatively few sites were available; in such cases, the Canberra region could be undersampled. To account for this, the analysis has been reported for both 1) all sites (all n) and 2) sites where $n > 30$ as can be seen in Table 1, which shows the limited difference between the two datasets. Where $n < 30$, this study only retains the events that were produced by mesoscale and synoptic-scale meteorological events similar to those that caused ramp events later in the dataset (where greater numbers of sites were present). Figure 2 shows that, despite the increase in reported site numbers with time, this has a limited effect on ramp-event identification (even when $n < 30$), as sites are geographically well dispersed for the entire period of study.

3. Results and discussion

Thirty-four critical collective ramp events that surpassed the specified ramp-rate threshold and were caused by repeatable, categorical weather phenomena were identified throughout the period of study (with approximately one event occurring each month), 18 of which were positive and 16 of which were negative. The weather categories associated with positive and negative ramp events are presented below. Table 1 shows the frequency and season of the weather types that caused the positive and negative ramp events. Table 2 presents the ramp rates associated with each individual ramp event. Overall, the average ramp rates of positive (70.3% of clear-sky potential) and negative (71.0% of clear-sky potential) events are very similar; however, it should be noted that when non-reoccurring weather events (the ''other'' category in Table 2) are ignored for both positive and negative ramp events, negative ramp events exhibit a slightly stronger ramp rate (positive, 69.9%; negative, 74.3% of clear-sky potential). Distinct differences between different types of weather events causing ramp events are observed (see Table 1), and so each reoccurring weather type is discussed next.

a. Positive ramp events

Eighteen positive ramp events occurred throughout the study period, with the majority of positive ramp events occurring prior to solar noon. The weather events that caused positive ramp events are discussed below, beginning with the most frequently occurring weather types.

1) NORTHWEST CLOUD BANDS

The northwest Australian cloud band frequently occurs in winter, when low-level stratiform cloud forms over northwest Australia, stretches across central Australia, and continues to the southeast, with cloud height progressively increasing. Cloud bands often extend over 5000 km, with a longitudinal length of up to 70° and a latitudinal length of 5°–10°. Moisture for the cloud band is usually provided by moist, deep convective cloud over the East Indian Ocean (Tapp and Barrell 1984; Sturman and Tapper 2005).

This paper draws a novel distinction between two types of northwest cloud bands, each of which induced a

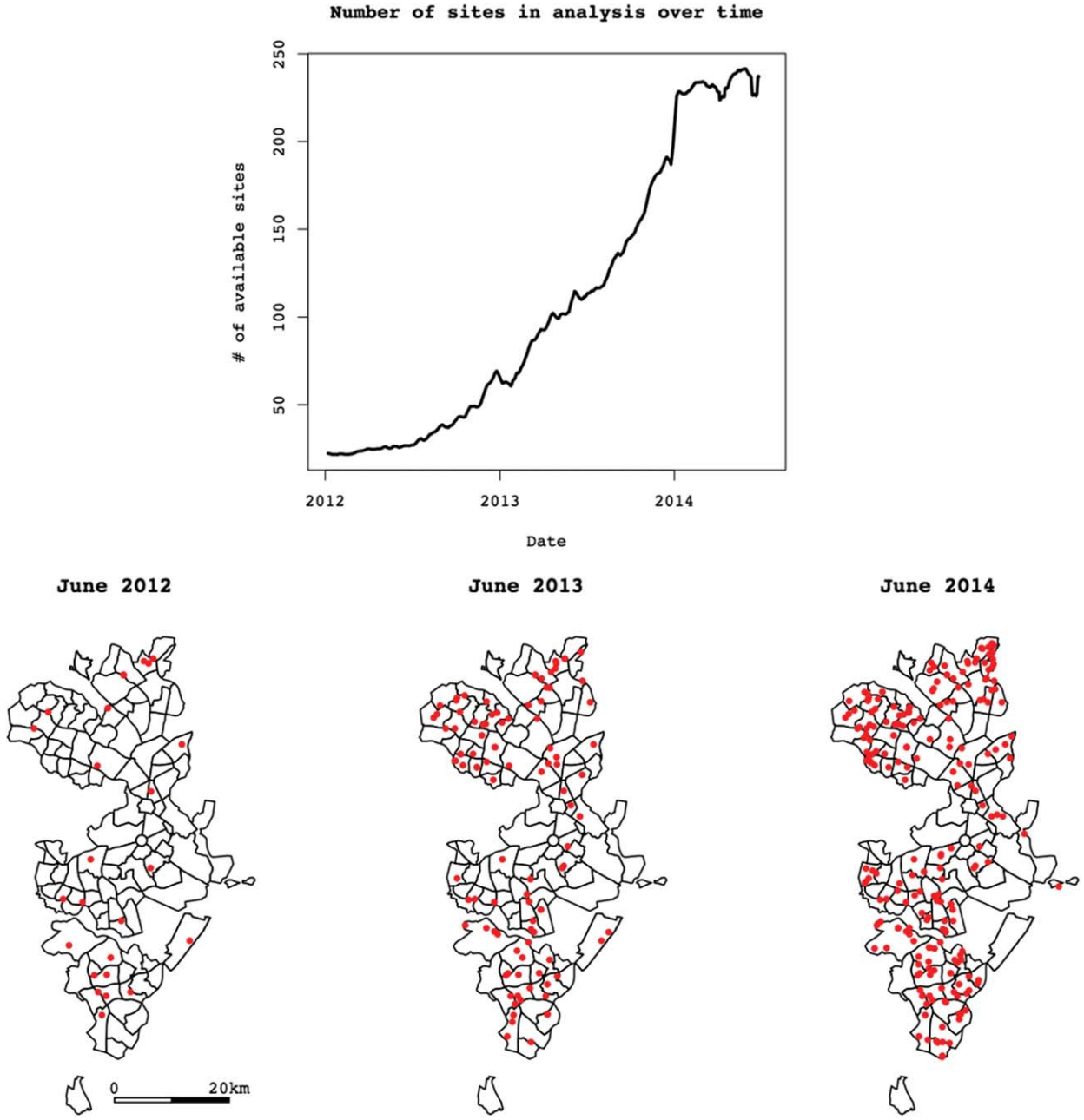

FIG. 2. (top) The total number of PV sites in Canberra available and used for analysis over time, beginning with 2 Jan 2012 and ending with 17 Jul 2014. (bottom) The geographic dispersion of sites across the ACT for 1 Jun (left) 2012 ($n = 27$), (center) 2013 ($n = 115$), and (right) 2014 ($n = 220$). As n increases with time, the spread of sites remains relatively constant throughout the period of analysis; the area of analysis increases from ~700 km^2 at the beginning of 2012 to ~800 km^2 in mid-2014. This shows that, even when $n < 30$, ramp events are caused by citywide, mesoscale, or synoptic-scale events.

different type of ramp event. We term the first type *synchronous* northwest cloud bands. These events occur when the cloud band's component synoptic features align: the southeastward-extending cloud band aligns with clouds generated by isentropic lifting that are associated with a low pressure system located off southeastern Australia and its incipient cold front (see Fig. 3). The merging of these two sources of cloud condensate produces a singular, clearly defined and well-developed cloud band that extends from the low levels to the midtroposphere (note the saturation at the 500-hPa level in Fig. 4). These well-developed cloud

TABLE 1. The different weather types that produced positive and negative ramp events in the ACT between January 2012 and July 2014. The frequency of ramp events induced by the given weather type is provided for both all observed ramp events regardless of the number of observation sites (n) and all ramp events when $n > 30$. This accounts for any potential bias due to the increase in the number of sites throughout the study period. The minimal difference between the columns shows that site number appears to have little impact on results, although this can only be determined with certainty with a longer time series. The average ramp event is quantified for each event type, both as a percentage of clear-sky potential exceeded within 60 min and as the change in PV output (kW kW_p^{-1}) [see Eqs. (1) and (2)]. The season in which each weather event occurred is also listed.

Weather event	Frequency (all n)	Frequency ($n > 30$)	Season	Clear sky (%)	kW kW_p^{-1}
Positive ramp events					
Northwest cloud band	5	4	November–March	74.5	0.526
Fog dissipation	4	2	April–August	64.1	0.374
Easterly dips and east coast lows	3	3	Dips: February Lows: May–June	62.6	0.417
Easterly trough	3	1	February	70.5	0.505
Cold front	1	0	September	77.8	0.423
Other	2	2	Various	72.1	0.388
Total	18	13		69.6	0.446
Negative ramp events					
Cold front	5	4	February–October	70.5	0.436
Thunderstorm	4	3	February–March; September	81.1	0.532
Northwest cloud band	3	3	November–December	78.4	0.380
Other	4	3	Various	60.8	0.391
Total	16	13		71.7	0.438

decks are most frequently associated with an upper-level trough, which supports surface regions of low pressure in southeastern Australia and accelerates the northwest-to-southeast moisture transport from the cloud band.

When the resulting opaque cloud deck moves out of the ACT, a positive ramp event occurs. There were three such events during the study period; the event from 20 December 2012 is shown in Figs. 4 and 5. The right-hand image in Fig. 4 shows the 500-hPa relative humidity in the 0000 UTC analysis from the ACCESS model, revealing a sudden drying at midlevels as the cloud band moves out of southeastern Australia. The cloud band it depicts is characteristically uniform, and shows a clear connection between its two synoptic components. This setup produced a sudden, strong ramp event at 0030 UTC 20 December 2012; as the cloud band moved out of the region, the aggregate power output from 67 PV sites jumped from 7.5% to 95% of clear-sky capacity in the hour preceding 0130 UTC (see Table 2).

In contrast, *asynchronous* northwest cloud bands (see Figs. 6 and 7) occur when the band's synoptic components do not align, producing two distinct, thinner cloud decks that are separated by a dry slotted region (Fig. 7). Interestingly, this asynchronous cloud band setup can lead to a series of positive and negative ramp events, as the frontal cloud region passes first, followed later by the cloud band after a period of clear sky. This occurred on two occasions throughout the study period. The asynchronous event of 15 November 2012 (Fig. 5) is presented with MSLP charts and satellite imagery in Fig. 6, which provides a clear example of this event type. A weak front is seen passing through southeastern Australia with relatively thin and scattered cloud cover, followed by a trailing cloud band. ACCESS model analysis reveals a disconnect in midtropospheric moisture, with an associated dry slot between the two features. The overall reduction in saturation at 500 hPa, compared to the more vigorous synchronous event, is noteworthy.

The difference in the overall moisture content and depth of the cloud formation is readily apparent in Fig. 5, which shows the contrast between the passage of the synchronous cloud band on 20 December 2012 and the asynchronous event on 15 November 2012. The synchronous event shows a greater overall reduction in solar radiation receipt, with less than 10% of clear-sky equivalent power production, and it produces a much stronger positive ramp event when conditions clear abruptly (see Table 2). The asynchronous event on 15 November 2012 produces three ramp events (two positive and one negative), with the first positive event commencing at 2230 UTC and the second at 0630 UTC 16 November 2012. Although only the first positive event meets the threshold for a critical event, it is nevertheless interesting to observe this phenomenon.

2) FOG DISSIPATION

Canberra experiences an average of 46 fog days per year, the majority of which are radiation fog events (Fabbian et al. 2007). Radiation fog typically occurs in the morning when light winds prevail, nights are clear,

TABLE 2. The date of each positive ramp event identified in this study. This includes the weather event type and the respective ramp quantified by the percentage change in clear-sky potential and the change in PV power output (kW kW_p^{-1}) as experienced over 60 min or less [see Eqs. (1) and (2)]. The number of sites used in the analysis is n.

Date	Event type	Clear sky (%)	kW kW_p^{-1}	n
7 Feb 2012	Easterly trough	60.7	0.388	22
10 Feb 2012	Easterly trough	86.7	0.704	22
17 Feb 2012	Northwest cloud band	78.3	0.607	21
27 Apr 2012	Fog	66.5	0.364	25
17 May 2012	Fog	65.0	0.413	25
13 Sep 2012	Cold front	77.8	0.423	38
15 Nov 2012	Northwest cloud band	81.0	0.520	48
20 Dec 2012	Northwest cloud band	87.5	0.623	67
2 Feb 2013	Easterly dip	65.2	0.397	72
31 Mar 2013	Northwest cloud band	61.3	0.363	92
26 Jul 2013	Fog	62.9	0.353	117
16 Aug 2013	Fog	62.0	0.369	126
31 Aug 2013	Other	81.8	0.490	136
28 Oct 2013	Other	74.2	0.320	158
28 Nov 2013	Northwest cloud band	64.5	0.516	183
11 Feb 2014	Easterly trough	64.1	0.422	191
2 May 2014	East coast low	60.1	0.421	240
15 Jun 2014	East coast low	62.4	0.432	239

and anticyclonic conditions are present (Fitzjarrald and Lala 1989; Meyer and Lala 1990). All four fog dissipation ramp events occurred between April and August, when a high pressure system was centered over either southeast or central Australia. The events are accompanied by a unique signal that is clearly detected by surface-level meteorological instruments: a lagged fall in relative humidity; a leading, sudden climb in temperature; and, throughout the event itself, an intensification in wind speed associated with an increase in turbulent mixing (and a sudden increase in PV power output). This signal, and the temporal relationship between its constituent elements, could be incorporated into future forecasts of fog dissipation ramp events. It is the signal *as a whole* that is of interest, rather than quantifying the intricate relationships between the parameters (e.g., the exact lag and lead times of each parameter and solar irradiance). While changes in certain parameters can be used to predict fog dissipation events, the lead time of such forecasts is short. Consequently, we are most interested in quantifying the feature vector "signature" of a fog dissipation event so that it can be incorporated into longer-term ML forecasting algorithms.

We use the ramp event of 17 May 2012 as an example. A favorable setup exists prior to the ramp: wind speeds are minimal and an anticyclone is dominant. These conditions promote overnight diabatic cooling. Consequently, the temperature of the prevailing air mass drops overnight and low temperatures (0°–2°C) are recorded until approximately 2100 UTC, when the air mass reaches saturation and radiative fog forms. After sunrise, the ground surface begins to warm, producing weak convection that begins the process of low-level mixing and fog dissipation. This process is a positive feedback cycle: as more mixing occurs, conditions clear, allowing more radiation to arrive at the surface, which further intensifies mixing. Figure 8 shows the response in collective PV power output ($n = 27$), which rises very suddenly, with a corresponding sudden fall in relative humidity. As the number of sites reporting this event was low ($n = 27$), additional analysis was completed to determine if this event occurred at the local or mesoscale. The wide distribution of sites (very similar to Fig. 2, bottom left), coupled with the appearance of the ramp-event signal in the geographically dispersed stations (see Fig.8) shows that the ramp event occurred across the Canberra region and is a mesoscale event.

Because radiative fog formation is dependent on diurnal heating, it is very likely positive fog dissipation ramp events will occur in the morning. Importantly, these events will not take place overnight, and so PV output will always be affected. Radiation fog dissipation is "fixed" temporally, contributing to the high frequency of radiative fog dissipation positive ramp-event observations. We also note that the strength of this ramp-event type can be diminished in the presence of upper-level cloud, which reduces the intensity of incoming radiation. Both of these points should be incorporated into any future feature vectors developed for radiation fog dissipation.

3) EASTERLY DIPS AND EAST COAST LOWS

As easterly dips and east coast lows originate under similar conditions, they are discussed here in tandem. Easterly dips may develop either onshore or offshore. The former develop when the quasi-stationary easterly trough (discussed in greater detail in the next subsection), located to the east of the Great Dividing Range, moves eastward and is either accompanied by a surface cutoff low or by upper-level northwesterlies ahead of a short wave. Offshore easterly dips occur when a quasi-stationary trough lies parallel with the east Australian coast, and is accompanied either by an advancing short wave or a 500-hPa cutoff low (Speer and Geerts 1994). Occasionally, an offshore easterly dip may develop into an east coast low. An east coast low is a particular category of extratropical cyclone that develops offshore within 500 km of the east Australian coast,

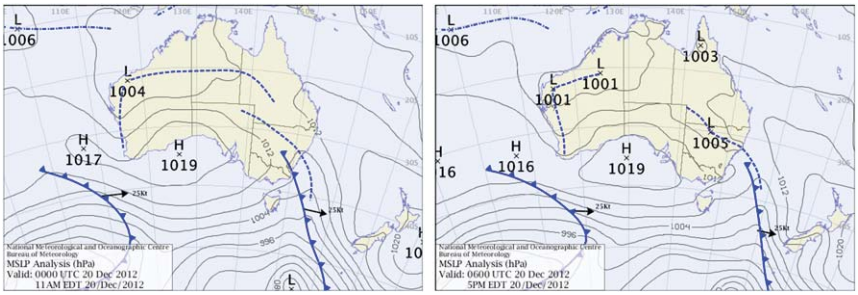

FIG. 3. MSLP charts showing conditions on 20 Dec 2012 when a positive ramp event was experienced over the ACT at approximately 2310 UTC. Shown are conditions at (left) 0000 and (right) 0600 UTC. These charts show that the synoptic surface features composing the northwest cloud band (the continental trough and cold front) are closely aligned. (Images are from the BoM.)

between 20° and 40°S latitude. They must display a degree of meridional movement throughout their lifetime and possess a pressure gradient of at least 4 hPa $(100\,\text{km})^{-1}$ (Holland et al. 1987; Hopkins and Holland 1997). Throughout the period of study, one easterly dip and two east coast lows produced morning positive ramp events; these types of events produce low- to midlevel strength ramp events (see Table 2).

We present the easterly dip positive ramp event on 2 February 2013 in Fig. 9, which shows conditions as the ramp began at 0000 UTC. The right-hand satellite image shows that a rapid decrease in cloud cover, connected with the easterly dip that is moving farther offshore as cyclogenesis intensifies, will soon be experienced over southeastern Australia. The left-hand thickness chart shows a distinct short-wave feature over the Victorian and New South Wales coasts, increasing cyclonic vorticity and enabling the surface low to deepen. The ramp event occurred as the offshore low pressure system and its associated cloud moved eastward.

4) EASTERLY TROUGH

The easterly trough (or "Queensland trough") is a semipermanent shallow region of low pressure that stretches meridionally in parallel with, and approximately 700 km inland from, the east coast of Australia. The easterly trough forms in response to (i) orography, (ii) diurnal heating, and (iii) the baroclinic zone originating from the contrasting temperatures of the land surface and the oceanic East Australian Current. It is often observed in summer, when maximum daytime heating occurs. The easterly trough divides moist, maritime air from dry, continental air. As surface heating increases throughout the day, mixing of the lower troposphere also increases, and the surface air to the west of the trough dries. As the trough deepens, it moves

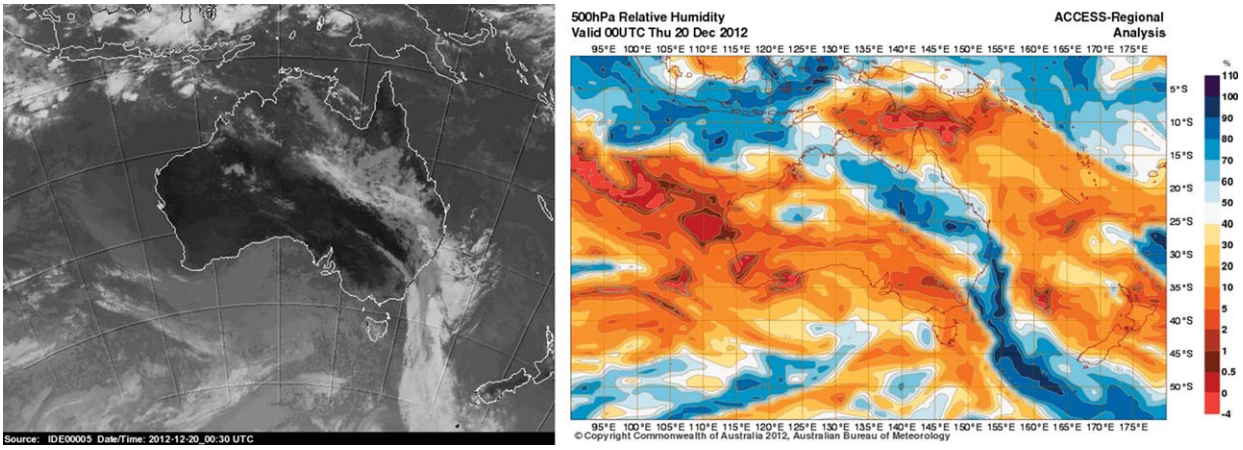

FIG. 4. Conditions at approximately 0000 UTC 20 Dec 2012, the time at which a positive ramp event commenced over the ACT. (left) Satellite image revealing the cloud band as it moves out of southeastern Australia (2310 UTC). (right) Image showing the 500-hPa humidity (%) analysis time step from the BoM ACCESS model. (Images are from the BoM.)

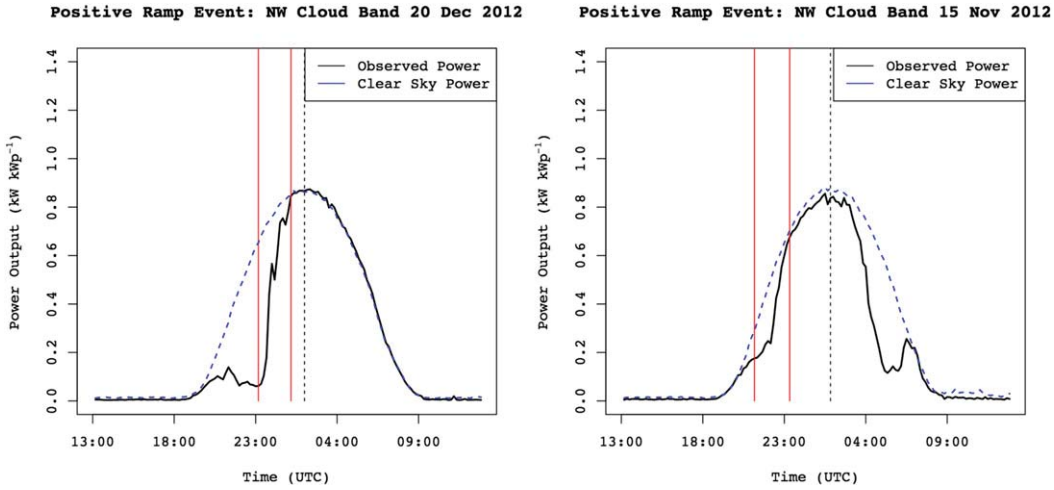

FIG. 5. The measured collective (n = 48 and 67, respectively) and clear-sky power output (kW kW_p^{-1}) of the available PV sites during positive ramp events associated with northwest cloud bands. (left) The synchronous event at 2310 UTC 20 Dec 2012 (bounded by the red vertical lines). (right) The asynchronous event at 2210 UTC 15 Nov 2012 (bounded by the red vertical lines), caused by the passage of frontal cloud, can be seen. Additionally, both a (critical) negative and a (noncritical) positive ramp event are observed in the afternoon of this day (at 0400 and 0600 UTC, respectively) as the northwest cloud band passes. The black dashed vertical line indicates midday.

eastward; this often prompts afternoon showers and thunderstorms (Adams 1986).

Throughout the period of study, three easterly trough positive ramp events were observed, all of which occurred in February (late summer). Two of these ramp events occurred solely as a consequence of changes in cloud produced by the easterly trough. One such trough occurred on 10 February 2012, as convective cloud generated by the easterly trough passed over the ACT, producing both a negative (0400 UTC) and a positive (0500 UTC) ramp event (see Fig. 10).

Weaker easterly troughs that do not stretch meridionally from Queensland through to Victoria may still produce ramp events when occurring in conjunction with other meteorological phenomena. One example occurred on 11 February 2014, when a decaying cold front (located over the Tasman Sea) fed moisture into the anticyclonic flow of a high pressure system, located off the east Australian coast (see Fig. 11). The steep 850-hPa moisture gradient between the maritime air and the dry continental air (associated with a weakly developed easterly trough located in inland New South Wales), produced shallow convection. The moisture gradient is only visible at 850 hPa, as the weak easterly trough and the decaying cold front are both shallow features (see Fig. 11). A lack of upper-level support produced localized, low-level cloud over the ACT. The positive ramp event occurred as the moisture gradient moved eastward, in response to both the cold front decaying, and surface heating increasing. Because this ramp event was not due solely to an easterly trough, but by factors additional to diurnal heating, the event occurred in the morning.

5) COLD FRONTS

Cold fronts affecting southern Australia differ from those elsewhere in the world. First, they are often associated with prefrontal troughs that migrate ahead of the front, which may be coupled with a cold change [see section 3b(1) for a more detailed discussion] (Hanstrum et al. 1990). Second, the cold fronts tend to lack upper-level baroclinicity; third, the cold fronts interact with other low-latitude phenomena in various ways (an example of which is the northwest cloud band, in which the cold front interacts with a continental low pressure trough) (Sturman and Tapper 2005).

Although only one cold front (13 September 2012) produced a positive critical ramp event during the period of study, it is included here because of the high frequency with which cold fronts occur in southeast Australia, and the subsequent likelihood of repetition, as well as the relative ramp-rate strength it exhibited (77.8% of clear-sky capacity; see Table 2). The cold front occurred on 13 September 2012 and produced a strong positive ramp event when the cloud associated with the front moved eastward. Figure 12 depicts conditions prior to the ramp event, which commenced at 0200 UTC. The prefrontal trough typical of Australian cold fronts is observed in the MSLP chart. Figure 13 provides further insight, with the collective power output (n = 38) showing a sudden increase in PV output associated with the passage of the thick cloud deck. The

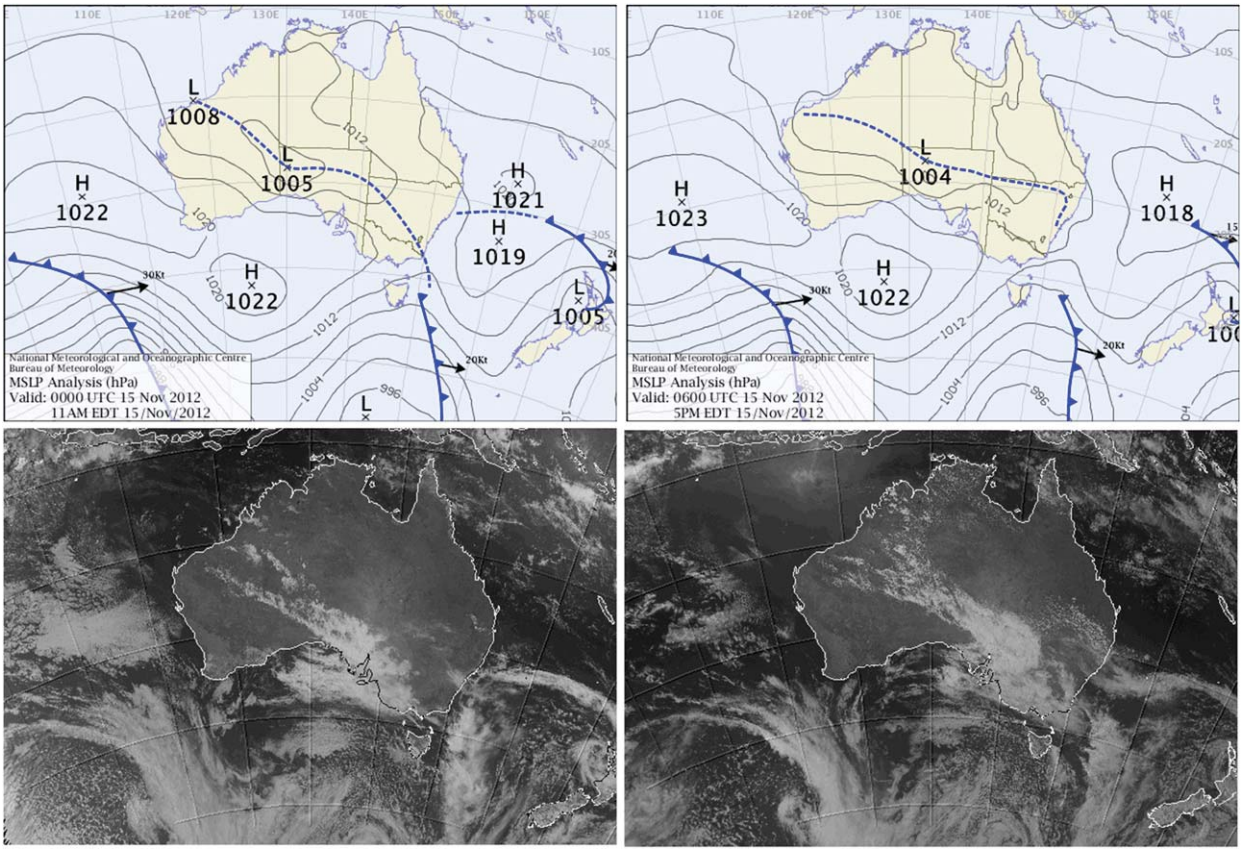

FIG. 6. Conditions on 15 Nov 2012 when the ACT underwent two positive ramp events due to the passage of an asynchronous northwest cloud band. Conditions are shown (left) at 0000 UTC when cloud associated with the leading cold front leaves the region and (right) at 0600 UTC when the arriving cloud band obscures the study area. (Images are from the BoM.)

arrival of the front at 0000 UTC is clear, with a drop in temperature and shift in wind direction. Temperatures rebound when the cloud clears a few hours later, before falling as a result of postfrontal cold-air advection.

It is possible that, despite their frequent passage across southeast Australia, few midlatitude cyclones result in positive ramp events because of the tendency of the associated cold fronts to make landfall with the southeast Australian coast in the afternoon and evening (Physick 1988). This situation would ordinarily cause cloud to clear overnight, as the resulting upshear cloud usually trails behind the surface front (and PV output remains unaffected). However, in this case, the blocking high located over the Tasman Sea on 13 September 2012 slowed the eastward movement of the cold front, enabling the midday ramp event.

b. *Negative ramp events*

A total of 16 collective negative ramp events surpassing the specified ramp-rate threshold were identified throughout the period of study and are placed into three categories: cold fronts, thunderstorms, and northwest cloud bands. Eleven of these were experienced in the afternoon. The bottom portion of Table 1 shows the frequency and season of the weather types that produced the negative ramp events. Each weather category is discussed below, beginning with the most frequently occurring weather type.

1) COLD FRONTS

There were four instances in which cold fronts resulted in negative ramp events throughout the period of study. The predominantly observed weather pattern was a surface anticyclone over the Tasman Sea, which produced northerly flow ahead of the cold front, and which then generated northwesterly flow as the front (and the coinciding ramp event) approached. This is exemplified by the event presented in Fig. 14, which shows a negative ramp event ($n = 148$) on 13 October 2013.

The particular characteristics of southern Australian cold fronts were discussed in section 3a(5). Fronts in the Australian region are often associated with prefrontal troughs, which migrate at the surface ahead of a midlatitude system. Prefrontal troughs embedded in

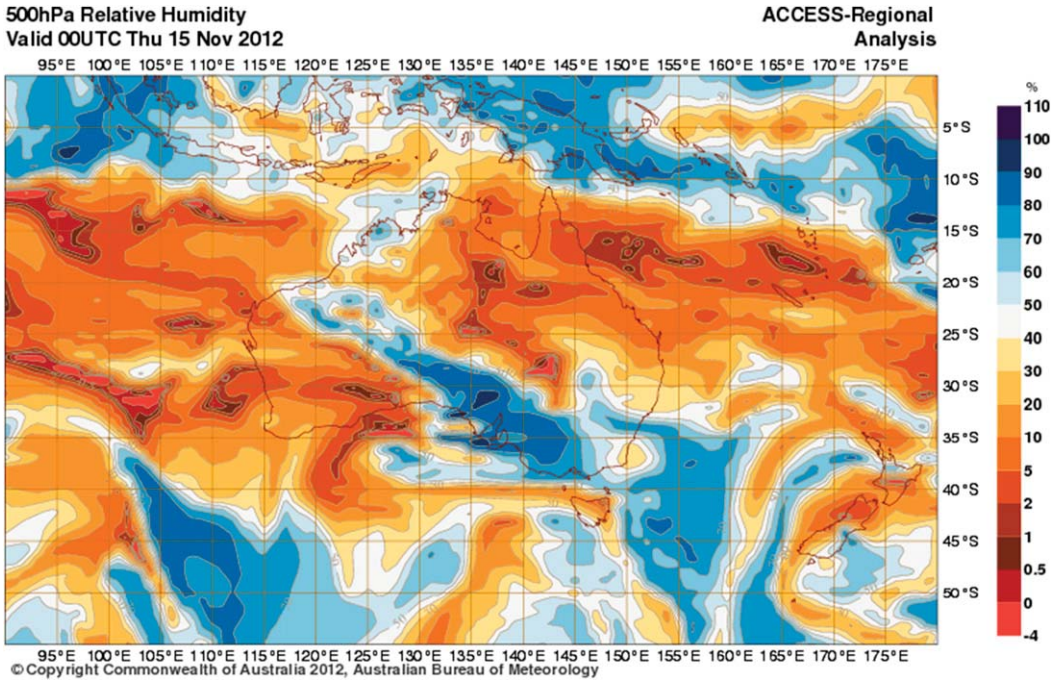

FIG. 7. Relative humidity (%) at 0000 UTC 15 Nov 2012 for the 500-hPa level, as determined by the ACCESS model initialization (Image is from the BoM.)

westward flow are known as ''westerly troughs'' and are often associated with a cold front stretching northward from the Southern Ocean. Westerly prefrontal troughs can develop into deep baroclinic systems and often produce a moderate cool change ahead of an approaching front (Hanstrum et al. 1990; Sturman and Tapper 2005). Figure 15 shows a well-developed westerly trough with a weak prefrontal cloud band.

Negative ramp events induced by cold fronts were typically associated with either a prefrontal westerly trough or a secondary cold front (located to the west, behind the first cold front). Consequently, such ramp events were initiated by low- to midlevel cloud produced by surface convergence along the prefrontal trough and, then, maintained by deeper, stratiform cloud layers developing upshear of the following cold front, producing zonally broad cloud decks (see Fig. 15). Given the observed climatological tendency for fronts with broad cloud decks to arrive in the late afternoon, overall PV output was likely to remain low after a ramp event occurred, as cloud would not pass until after nightfall. The predisposition of cold fronts to arrive in the afternoon or evening was discussed in section 3a(5) (Physick 1988). All recorded negative cold front ramp events occurred after midday.

2) THUNDERSTORMS

Thunderstorms occur when the atmosphere undergoes rapid destabilization via convection; the cause of this destabilization varies geographically across Australia. While storms in northern Australia often develop as a result of intense surface heating, southeast Australian summer storms may result from westerly cool changes or from warm, moist flow into surface troughs. In winter, storms are primarily associated with

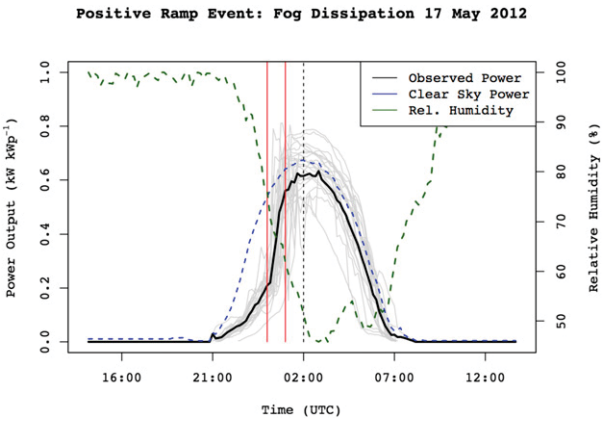

FIG. 8. Fog dissipation positive critical ramp event (bounded by the red vertical lines and occurring at 0000 UTC) of 17 May 2012 using data reported from a collective of 27 individual sites. Plotted are the collective and clear-sky power output (kW kW_p^{-1}) and the relative humidity (%) vs UTC time stamps. The black dashed vertical line indicates midday. The gray lines show the PV output from each of the geographically dispersed 27 sites. The majority of sites exhibit the ramp-event signal, which indicates that the fog event was a mesoscale event.

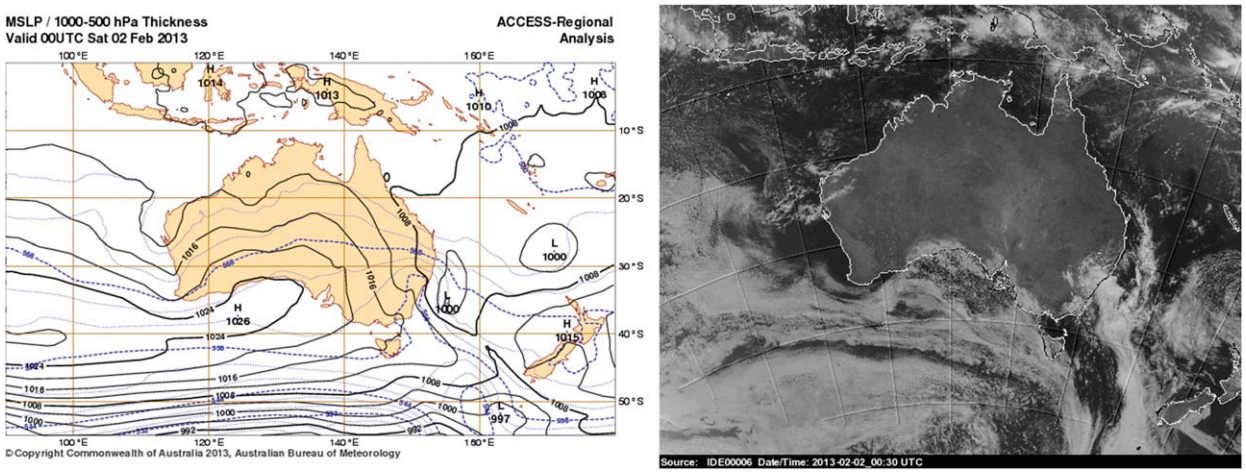

FIG. 9. Conditions at 0000 UTC 2 Feb 2013. (left) The 1000–500-hPa thickness shows 1000-hPa isohypes in black and 500-hPa isohypes in dashed blue. (right) Satellite cloud image at 0030 UTC. (Images are from the BoM.)

the passage of cold fronts (Sturman and Tapper 2005; Australian Bureau of Meteorology 2014). Four thunderstorm-induced ramp events were observed, which produced distinct signals in the collective PV power output and meteorological records. The most notable event was the negative ramp event (n = 234) that occurred on 19 February 2014, which was generated by the arrival of thunderstorm anvil downshear at 0030 UTC. This event was followed by a continued drop in PV power production to levels less than 10% of the clear-sky potential. Thereafter, an initial fall in surface pressure and then a pronounced rebound (along with a drop in temperature) occurred with the arrival of the cold pool and mesohigh, as indicated clearly by the rising pressure in the bottom panel of Fig. 16, as well as the increased wind speed, shifting wind direction, and falling temperature, which coincide with the arriving gust front and occur within the space of several hours. This cold

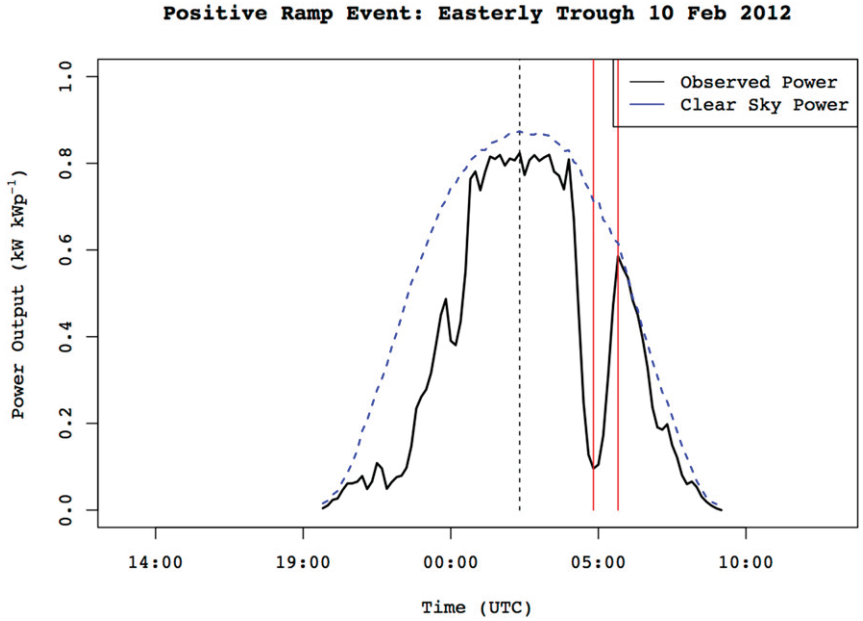

FIG. 10. The negative (0400 UTC) and positive (0450 UTC, bounded by the red vertical lines) ramp events of 10 Feb 2012 caused by the passage of convective cloud generated by an easterly trough. The event was determined using data reported from a collective of 22 individual sites. Shown is the collective and clear-sky potential power output (kW kW$_p^{-1}$) plotted against UTC time stamps. The black dashed vertical line indicates midday.

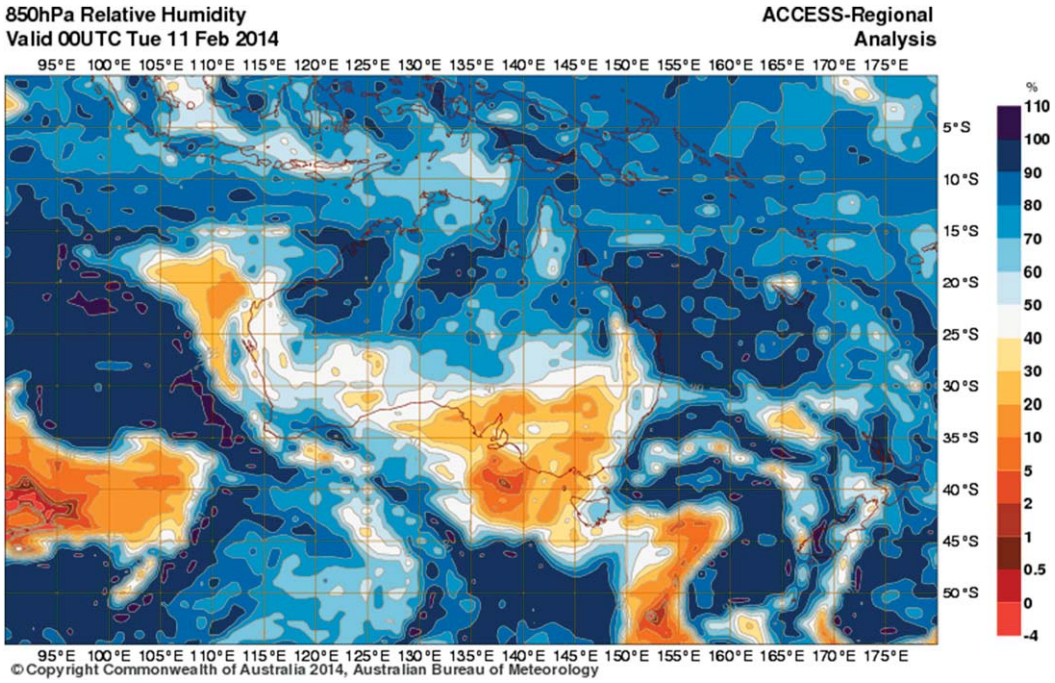

FIG. 11. The 0000 UTC ACCESS model 850-hPa relative humidity (%) analysis of 11 Feb 2014. A sharp moisture gradient at low levels dividing the continental and maritime air masses, centered above the easterly surface trough, is revealed. (Image is from the BoM.)

pool and mesohigh signal differentiates thunderstorm events from other low pressure events (Engerer et al. 2008) and is clearly present in Fig. 16. This is followed by an extended period of reduced power output.

Further investigation into the meteorological origins of the thunderstorm responsible for this event revealed a weak surface low moving into an embedded easterly trough. This is apparent in Fig. 17, which shows conditions at 0000 UTC, approximately 30 min prior to the negative ramp event. The ramp event coincides with advection of the thunderstorm anvil from the northwest, seen clearly in the right-hand image of Fig. 17.

3) NORTHWEST CLOUD BAND

Three synchronous northwest cloud bands contributed to negative ramp events throughout the period of study. In each case, the northwest cloud band was connected to a midlatitude cyclone in the southeast as a single, broad cloud feature. A negative ramp event may occur if the forward boundary of this cloud band is homogeneous and sufficiently opaque, or if thin, high-level clouds precede a thicker, suddenly arriving stratus deck. Figure 18 shows the changes in PV output accompanying the latter event type; thin clouds are present before

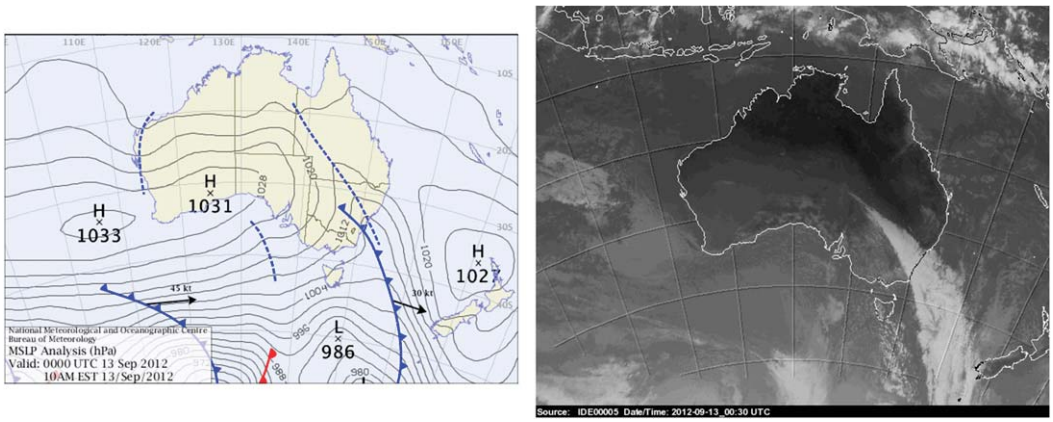

FIG. 12. Synoptic conditions at (left) 0000 and (right) 0030 UTC 13 Sep 2012. (Images are from the BoM.)

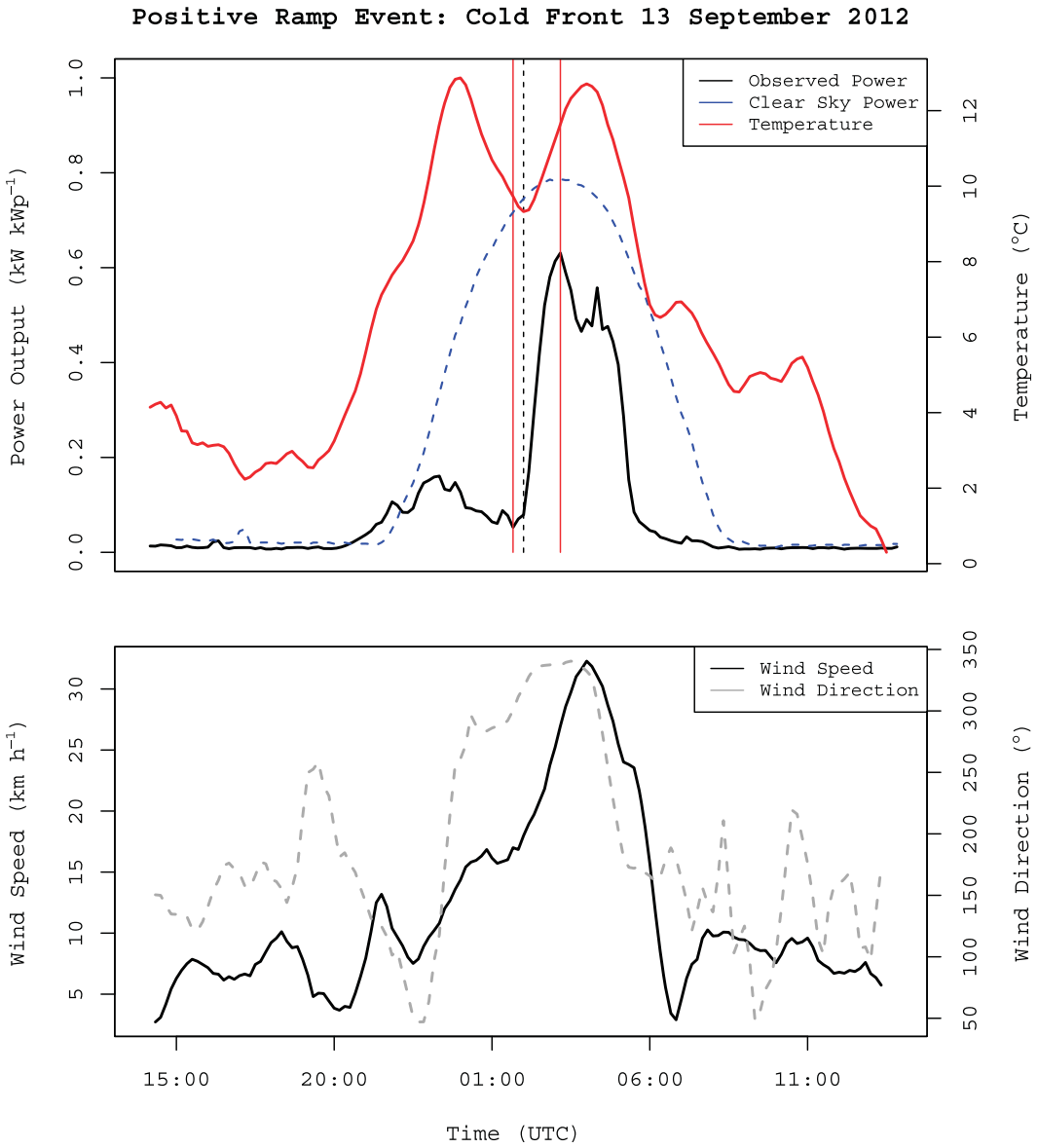

FIG. 13. The PV output and meteorological observations associated with the collective positive ramp event that occurred on 13 Sep 2012 (beginning at 0150 UTC and bounded by the red vertical lines; the black dashed vertical line indicates midday). (top) The PV output (black; $n = 38$) and clear-sky potential (blue) (kW kW$_p^{-1}$), along with the ambient temperature (°C; red). (bottom) The observed wind speed (black solid) and direction (gray dashed). The passage of a cold front is apparent just after 2300 UTC when a sudden drop in temperature and shift in wind speed is observed. This is followed by a positive ramp event at 0150 UTC and a rebound in temperature associated with the clearing cloud.

incoming radiation is suddenly reduced with the arrival of a thicker layer of cloud. An exemplary event occurred on 9 December 2013, when a departure from clear-sky potential was apparent prior to the ramp event, indicating the presence of thin, upper-level clouds. These features are apparent in the satellite image presented in Fig. 19. A thicker layer of cloud arrives at approximately 0300 UTC, accompanied by a sudden reduction in collective PV power output ($n = 188$). The 500-hPa relative humidity analysis from the ACCESS model in Fig. 19 shows an area of increased midlevel moisture content. This is further supported by the apparent thickening of cloud in the satellite image from 0000 UTC.

c. *Further discussion*

When presenting and categorizing the meteorological phenomena that cause critical ramp events, it is a natural follow-on investigation to identify how often these

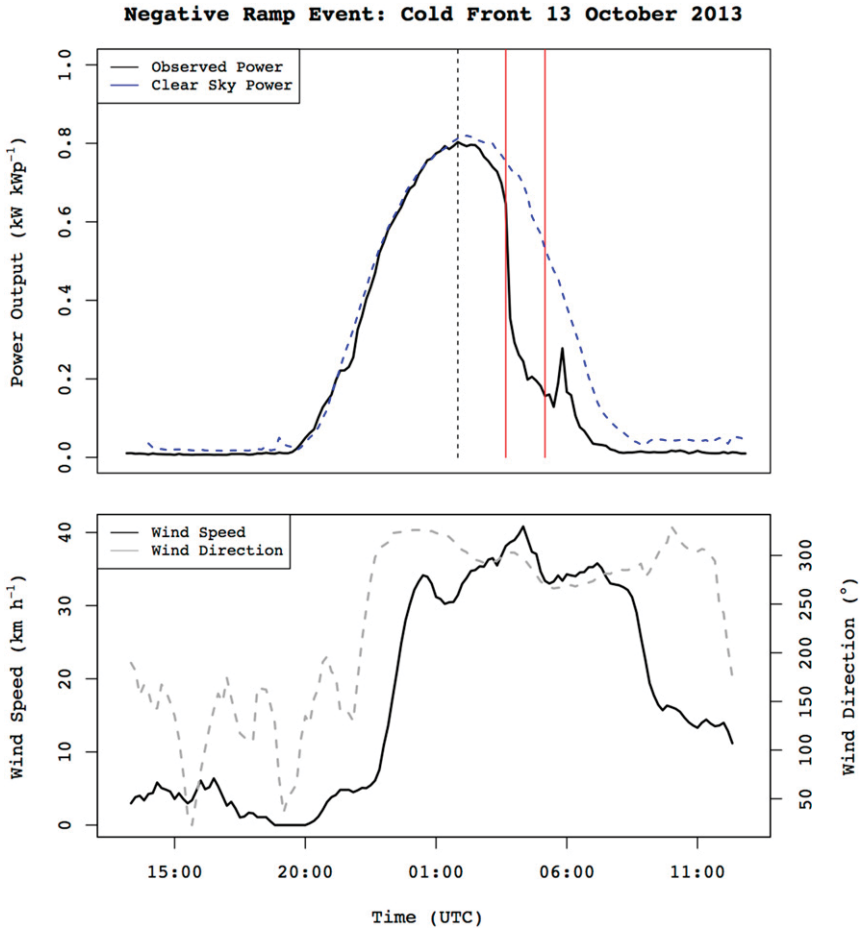

FIG. 14. (top) The measured collective PV output (black; $n = 148$) and clear-sky potential (blue) from a negative ramp event associated with a cold front on 13 Oct 2013. The ramp event began at 0440 UTC and is bounded by the red vertical lines, and the black dashed vertical line indicates midday. (bottom) Selected observations that show wind speed (solid black; km h^{-1}) and wind direction (dashed gray; °).

categorized events occurred but did not cause a critical ramp event. It is beyond the scope of this research to develop a climatology of these events to determine how critical and noncritical events differ, but this would be a useful counterpart to the current study. There should be a future focus on the distinction between noncritical and critical events in each category. Undertaking this analysis requires a climatology of the location of interest to have been developed previously; many of the weather categories discussed in this paper have not yet been formally studied in the ACT region, which makes conducting such an analysis difficult. Despite this limitation, some insights may be gathered from a basic analysis on weather types that have been examined in the ACT. Consider that there are, on average, 46 radiation fog events in Canberra annually (Fabbian et al. 2007), with only four of these events exceeding the critical threshold in an 18-month period. Even if the study period had uncharacteristically low numbers of fog events, this would still represent only a small portion of the observed fog events. This suggests that there are several factors that drive the rate of fog dissipation locally that warrant further investigation. For example, the geographic dispersion of sites likely plays an important role; in order for a critical ramp event to occur, fog must be both widespread and dissipating rapidly over the majority of monitored sites. Another point is that fog may dissipate more slowly in the presence of other layers of cloud, meaning that not all fog events result in rapid, widespread dissipation events.

This type of analysis carries over into the other categories. For example, thunderstorms are another weather type for which information, although somewhat coarse, is available in the ACT. On average, the ACT experiences approximately 20 thunder days annually (Kuleshov et al. 2002). Four thunderstorm-induced

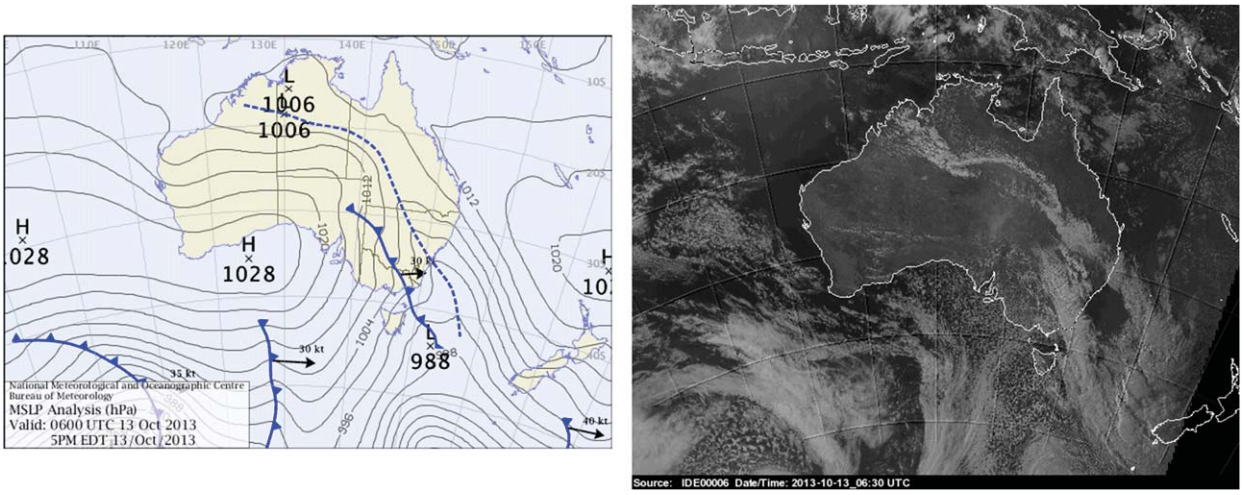

FIG. 15. (left) The MSLP chart showing conditions at 0600 UTC 13 Oct 2013, which is an hour after a cold-front-induced negative ramp event commenced. (right) The corresponding satellite image showing conditions at 0630 UTC. These two panels show how the cold front and prefrontal trough can produce a singular broad cloud deck that produces sudden, long-lasting reductions in PV power output. (Images are from the BoM.)

critical ramp events were recorded over this 30-month study period, which suggests that approximately 10% of thunderstorm events in the ACT result in critical ramp events. As little detail exists on different thunderstorm types affecting the ACT, it is difficult to posit why some thunderstorm events results in critical ramp events while others do not; a more extensive climatology of the ACT region needs to be developed before this relationship can be understood. Once this climatology is developed, further questions can be asked about this, and other, weather types. Perhaps only thunderstorm events with very little preexisting cloud cover lead to critical ramp events. Perhaps the presence of thin upper-level clouds reduces the impact of an approaching cold front. There are many avenues for future investigation, which would be valuable to pursue. But the absence of these answers in the present study does not detract from the value of first identifying the weather events that cause the critical ramp events, for without this initial analysis, the follow-on questions could not be posed, and neither could ML algorithms to forecast ramp events be developed that rely on the precategorization of weather types (e.g., Wong et al. 2008).

Another important factor determining whether one of the categorized weather events results in a ramp event is the time of day at which it occurs. Several features, such as easterly troughs and fog dissipation, are restricted to daytime occurrence, as a result of their dependence on diurnal heating. However, events such as east coast lows and cold fronts may occur at any time. These weather types only result in ramp events when they produce sudden cloud cover changes during the day. For example, the cold front that induced a positive ramp event on 13 September 2012 occurred because a blocking high slowed its eastward progress, allowing a departure from the climatological average of late afternoon and evening arrivals. We also observe a bias for positive critical ramp events to occur in the morning, and negative ramp events to occur in the afternoon and evening.

There is value in discussing the differences in ramp rates—that is, how quickly a ramp event occurs—between the different categories. While all ramp events surpassed the required threshold of 60% change in PV power output within 60 min, with respect to the clear-sky potential, the ramp rates varied according to weather type (see Tables 1–3). For example, the ramp rates associated with passing thunderstorms (77.0% of clear-sky potential within 60 min) tended to be higher than those associated with fog dissipation events (64.1% of clear-sky potential within 60 min), and synchronous northwest cloud band ramp events exhibited higher ramp rates than asynchronous events. This seems to suggest a direct relationship between increased cloud opacity and increased collective ramp rate. This reflects the time taken for each ramp event to occur; for example, fog dissipation events happen less quickly than thunderstorm ramp events. Differences in ramp rates additionally seem to suggest a direct relationship between increased cloud opacity and increased collective ramp rate. Differences between ramp rates measured as a percentage of clear-sky potential and as a change in PV output are occasionally visible [e.g., fog dissipation has a slightly higher percentage of clear-sky ramp rate

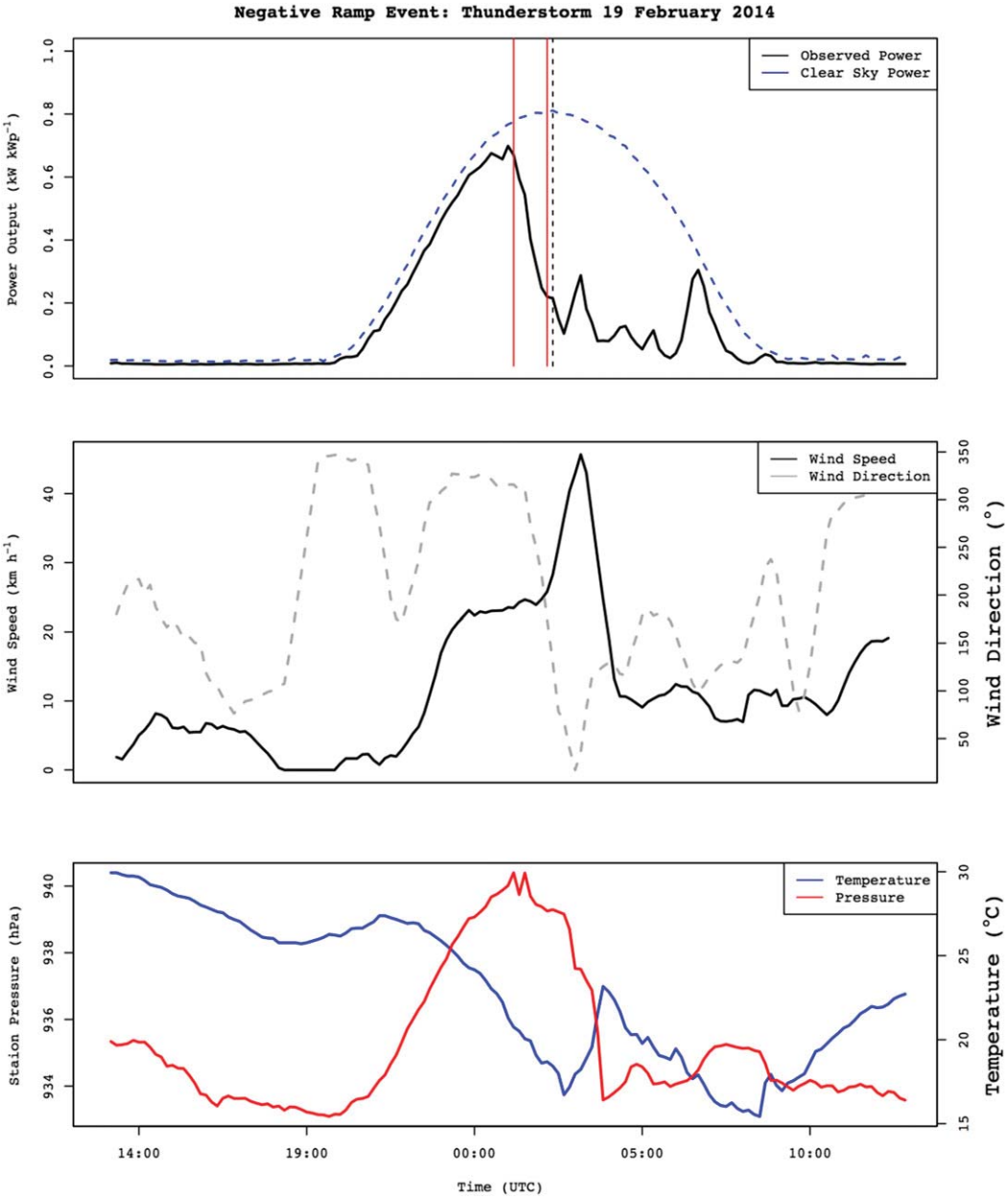

FIG. 16. The PV output and meteorological observations associated with the collective negative ramp event (n = 234) that occurred on 19 Feb 2014 (the ramp event begins at 0050 UTC and is bounded by the vertical red lines; midday is shown by the black dashed vertical line). (top) The PV output (solid black) and clear-sky potential (dashed blue) (kW kW$_p^{-1}$). (middle) The observed wind speed (solid black; km h^{-1}) and direction (dashed gray; °). (bottom) The station-level pressure (blue; hPa) and temperature (red; °C). A distinct mesohigh signal is apparent with the thunderstorm's passage, providing strong indications that the negative ramp event was caused by cloud from the thunderstorm anvil.

(64.1%) than do easterly dips and east coast lows (62.6%), while its change in PV output (0.374 kW kW$_p^{-1}$) is less than that of easterly dips and east coast lows (0.417 kW kW$_p^{-1}$); see Table 1]. This can be attributed to the time of day at which the ramp events occur. For example, the change in PV output is less for fog dissipation ramp events as they typically occur in the morning, when the potential for PV generational output is minimal.

There were several events that produced critical ramp events but that were not caused by phenomena deemed to be repeatable or able to be categorized (see the

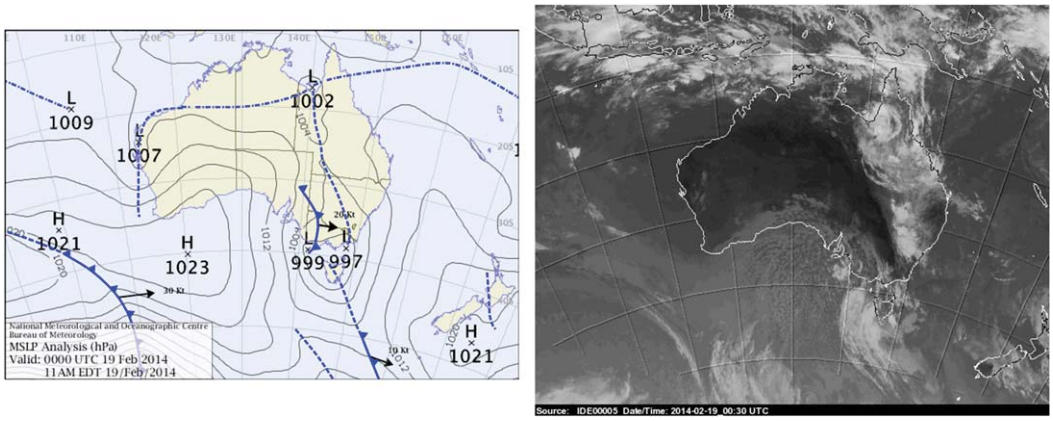

FIG. 17. Conditions on 19 Feb 2014. (left) The MSLP chart showing a meridional easterly trough with an approaching surface low, clearly providing the forcing mechanism required for initiating convection. (right) Satellite image showing the anvil cloud from an approaching convective storm being advected over the ACT region from the northwest. (Images are from the BoM.)

"other" category in Table 1). These were mostly caused by upper-level cloud features whose origins are challenging to define and were attributed to unique events such as the sudden dissipation of cloud under a low-level inversion. These events were not assigned categories because they occurred infrequently and were difficult to categorize (see the "other" category in Tables 1–3). As methods for automatically forecasting ramp events are likely to originate from systems that require prior categorization of the weather events of interest (e.g., Wong et al. 2008), the imperative to understand nonrepeating events is not as strong. That said, future follow-on work over longer time periods may conclude that these features should be included in the local climatology's ramp-event categorizations, but it is believed that doing so at this juncture would be premature.

4. Conclusions

This study has identified the meteorological origins of critical PV ramp events in the ACT region in southeastern Australia. We have proposed categories for these events based on an analysis of the phenomena that caused them. The categorization was completed with the premise in mind that the basic components of each of these events are repeatable and that therefore the categories are useful in applied meteorological methods. There are two primary areas in which these research results are particularly useful.

First, it has been demonstrated that the critical ramp events that occur in a region may be quite easily connected to repeatable meteorological phenomena. This suggests that future work should repeat this effort in other regions where high penetrations of distributed PV arrays are present, as these are the events most likely to cause widespread supply–demand balancing problems on the electrical grid. This could potentially increase the role of the local or regional meteorological authorities, who could serve as consultants to the energy industry, informing them of the likelihood of these events. Thereby, this paper provides a foundation on which PV ramp-event forecasts can be issued based on more traditional meteorological avenues (e.g., from a forecaster interpreting model output), rather than by (or in addition to) automated routines, which is the focus of modern research and current practice. The reader is invited to consider that "ramp event warnings" issued by an operational meteorologist to an energy market with very high penetrations of distributed PV could be very

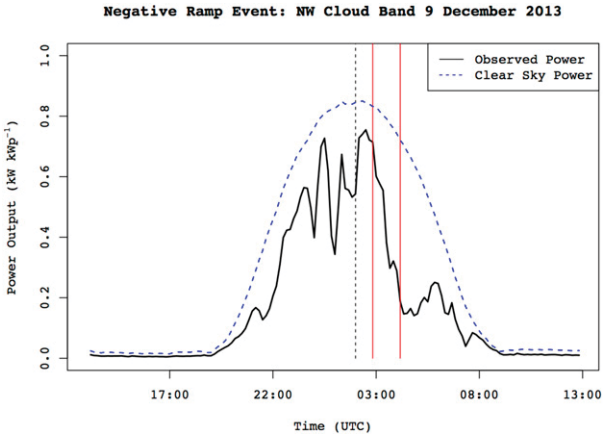

FIG. 18. Collective PV power output (n = 188) from 9 Dec 2013 when a northwest cloud band event caused a negative ramp event (indicated by the vertical red lines) in the ACT region. The ramp begins at 0250 UTC; the collective power output (black solid) and the clear-sky potential (blue dashed) (kW kW_p^{-1}) are shown. The black dashed vertical line indicates midday.

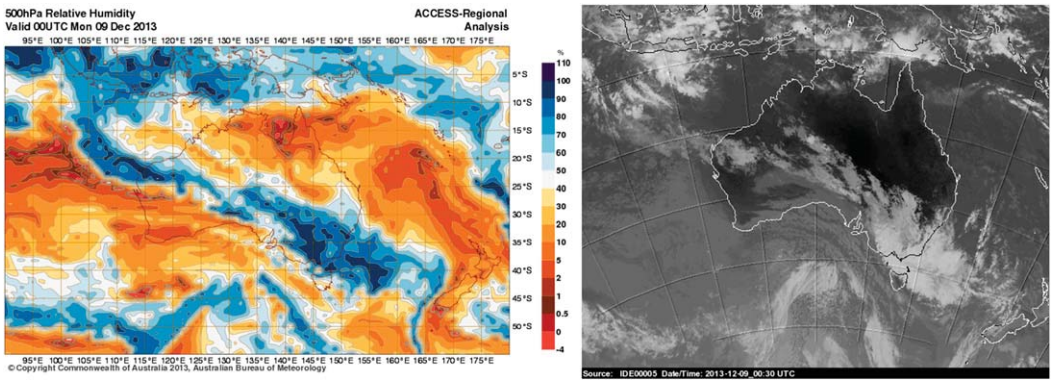

FIG. 19. (left) The 0000 UTC analysis from the ACCESS model showing relative humidity (%) at 500 hPa. (right) The satellite image from 0030 UTC. The model analysis and satellite image reveal a thick layer of midlevel cloud, following a thinner layer to the east. This thicker midlevel cloud was responsible for the negative ramp event.

valuable to entities involved in spot-market trading. That said, once these meteorological events are categorized, the possibility of automatic ramp-event detection becomes feasible (e.g., Wong et al. 2008). While such methods may initially be restricted to locations with repeating synoptic features, the development of such ML algorithms will likely allow for the future development of forecasting algorithms that detect nonrepeating weather types.

Second, it was originally hypothesized that this approach would provide possible avenues to address key weaknesses in current solar forecasting methodologies through automated weather categorization. That the ramp events identified were most often connected to repeatable synoptic and mesoscale meteorological events makes future work in this area more promising. For example, these findings could be used in short-term (<4 h) statistical methods, which have yet to properly leverage meteorological data in their forecasting routines (e.g., preprocessed feature vectors). Having identified that major, long-lived cloud features are often responsible for critical collective ramp events (e.g., northwest cloud bands, thunderstorm anvils), it is proposed that this may also be true for medium-term methods (4–8 h), which rely on satellite imagery, as well as long-term (>8 h) methodologies relying on numerical weather models.

A summary of the conclusions within the direct context of this paper alone is also relevant. We have discovered that the phenomena that produce critical collective ramp events in the ACT occur at the synoptic scale and the mesoscale. These events include cloud bands associated with cold fronts; easterly dips, lows, and easterly troughs; the rapid dissipation of radiation fog; the Australian northwest cloud band; and thunderstorms. Radiation fog events provide additional intrigue, as Canberra is particularly susceptible to this type of event. This suggests that local climatology is quite important when categorizing these events [supporting the conclusions of Boland (2015)] and that repeating this analysis in other cities would be useful. Second, there are some events, such as asynchronous northwest cloud bands and thunderstorms events, that can produce multiple negative and positive critical collective ramp events on the same day. Next, it has been found that critical ramp events occur when a rapid transition is made from clear skies to opaque cloud, and vice versa, as well as when thin cloud becomes opaque cloud, and vice versa.

Future work in this area will focus on discerning the characteristics that produce critical ramp events, and those that do not, for each meteorological category identified in this study. We also intend to repeat this

TABLE 3. As in Table 2, but for negative ramp events.

Date	Event type	Clear sky (%)	kW kW$_p^{-1}$	n
10 Feb 2012	Thunderstorm	86.7	0.704	22
1 Apr 2012	Other	60.2	0.527	25
5 Sep 2012	Cold front	88.2	0.491	38
18 Sep 2012	Thunderstorm	86.0	0.616	38
15 Nov 2012	Northwest cloud band	74.7	0.430	48
24 Dec 2012	Thunderstorm	77.0	0.263	61
9 Feb 2013	Cold front	63.7	0.461	69
20 Feb 2013	Other	60.8	0.399	76
29 Apr 2013	Cold front	60.7	0.312	96
22 Jun 2013	Other	61.7	0.377	112
13 Oct 2013	Cold front	76.7	0.519	148
28 Nov 2013	Northwest cloud band	82.0	0.400	183
9 Dec 2013	Northwest cloud band	69.8	0.311	188
19 Feb 2014	Other	60.5	0.262	234
30 Mar 2014	Thunderstorm	74.8	0.546	227
28 Jun 2014	Cold front	63.0	0.396	238

analysis in other capital cities in Australia, to discern the importance of local climatology on the categories presented. The authors are hopeful that similar work will be undertaken on this topic both in regional Australia and internationally. Further research aims to develop automated detection routines for the critical events detailed herein, so that they might be included as more useful inputs to modern statistical forecasting methods (e.g., as feature vectors to ML algorithms).

Acknowledgments. The authors thank the Australia Bureau of Meteorology for allowing its images to be reproduced, and for providing the meteorological data. They also thank the Australian Renewable Energy Agency (ARENA) for partially funding this research project through its U.S.–Australia Solar Energy Collaboration (USASEC) grant program. Author Engerer additionally thanks National ICT Australia for providing partial support for this project.

REFERENCES

Adams, M., 1986: A theoretical study of the inland trough of northeastern Australia. *Aust. Meteor. Mag.*, **34**, 85–92.

Australian Bureau of Meteorology, 2014: Storm spotters' handbook. [Available online at http://www.bom.gov.au/storm_spotters/handbook/foreword.shtml.]

Bing, J., P. Krishnani, O. Bartholomy, T. Hoff, and R. Perez, 2012: Solar Monitoring, Forecasting and Variability Assessment at SMUD. *World Renewable Energy Forum*, Denver, CO, American Solar Energy Society, 1–8.

Boland, J., 2015: Spatial-temporal forecasting of solar radiation. *Renew. Energy*, **75**, 607–616, doi:10.1016/j.renene.2014.10.035.

CEC, 2013: Clean energy Australia: Report 2013. Clean Energy Council, 73 pp. [Available online at https://www.cleanenergycouncil.org.au/dam/cec/policy-and-advocacy/reports/2014/Clean-Energy-Australia-Report-2013.pdf.]

Chel, A., and G. Tiwari, 2011: A case study of a typical 2.32 kW_p stand-alone photovoltaic (SAPV) in composite climate of New Delhi (India). *Appl. Energy*, **88**, 1415–1426, doi:10.1016/j.apenergy.2010.10.027.

Chen, C., S. Duan, T. Cai, and B. Liu, 2011: Online 24-h solar power forecasting based on weather type classification using artificial neural network. *Sol. Energy*, **85**, 2856–2870, doi:10.1016/j.solener.2011.08.027.

Detyniecki, M., C. Marsala, A. Krishnan, and M. Siegel, 2012: Weather-based solar energy prediction. *Int. Conf. on Fuzzy Systems*, Brisbane, QLD, Australia, IEEE, doi:10.1109/FUZZ-IEEE.2012.6251145.

Engerer, N. A., 2011: Simulating photovoltaic array performance using radiation observations from the Oklahoma Mesonet. M.S. thesis, School of Meteorology, University of Oklahoma, 225 pp.

——, 2013: Short-term machine learning based power output forecasts for collectives of rooftop photovoltaics. *Proc. Second Int. Conf. on Energy and Meteorology*, Toulouse, France, U.N. Office for Disaster Risk Reduction.

——, 2015: Minute resolution estimates of the diffuse fraction of global irradiance for southeastern Australia. *Sol. Energy*, **116**, 215–237, doi:10.1016/j.solener.2015.04.012.

——, and F. P. Mills, 2014: K_{PV}: A clear-sky index for photovoltaics. *Solar Energy*, **105**, 679–693, doi:10.1016/j.solener.2014.04.019.

——, and S. J. Wellby, 2014: Categorising meteorological events as inputs to machine learning based solar forecasts. *20th Annual Meeting of the Australian Meteorological and Oceanographic Society*, Hobart, Tasmania, AMOS.

——, and Y. Xu, 2015: A simple model for estimating the diffuse fraction of solar irradiance from photovoltaic array power output. *21st Int. Congress on Modelling and Simulation (MODIM2015)*, Broadbeach, QLD, Australia, Modelling and Simulation Society of Australia and New Zealand. [Available online at http://www.mssanz.org.au/modsim2015/M2/engerer.pdf.]

——, D. J. Stensrud, and M. C. Coniglio, 2008: Surface characteristics of observed cold pools. *Mon. Wea. Rev.*, **136**, 4839–4849, doi:10.1175/2008MWR2528.1.

Fabbian, D., R. de Dear, and S. Lellyett, 2007: Application of artificial neural network forecasts to predict fog at Canberra International Airport. *Wea. Forecasting*, **22**, 372–381, doi:10.1175/WAF980.1.

Fitzjarrald, D. R., and G. G. Lala, 1989: Hudson Valley fog environments. *J. Appl. Meteor.*, **28**, 1303–1328, doi:10.1175/1520-0450(1989)028<1303:HVFE>2.0.CO;2.

Florita, A., B.-M. Hodge, and K. Orwig, 2013: Identifying wind and solar ramping events. *Proc. Fifth Green Technologies Conf.*, Denver, CO, IEEE, 147–152.

Hanstrum, B., K. Wilson, and S. Barrell, 1990: Prefrontal troughs over southern Australia. Part I: A climatology. *Wea. Forecasting*, **5**, 22–31, doi:10.1175/1520-0434(1990)005<0022:PTOSAP>2.0.CO;2.

Hoff, T. E., and R. Perez, 2010a: Modeling PV fleet output variability. *Sol. Energy*, **86**, 2177–2189.

——, and ——, 2010b: Quantifying PV power output variability. *Sol. Energy*, **84**, 1782–1793, doi:10.1016/j.solener.2010.07.003.

Holland, G. J., A. H. Lynch, and L. M. Leslie, 1987: Australian east-coast cyclones. Part I: Synoptic overview and case study. *Mon. Wea. Rev.*, **115**, 3024–3036, doi:10.1175/1520-0493(1987)115<3024:AECCPI>2.0.CO;2.

Hopkins, L. C., and G. J. Holland, 1997: Australian heavy-rain days and associated east coast cyclones: 1958–92. *J. Climate*, **10**, 621–635, doi:10.1175/1520-0442(1997)010<0621:AHRDAA>2.0.CO;2.

Huang, J., M. Korolkiewicz, M. Agrawal, and J. Boland, 2013: Forecasting solar radiation on an hourly time scale using a Coupled AutoRegressive and Dynamical System (CARDS) model. *Sol. Energy*, **87**, 136–149, doi:10.1016/j.solener.2012.10.012.

IEA, 2013: Renewable energy outlook. World Energy Outlook, International Energy Agency Tech. Rep., 196–232. [Available online at http://www.worldenergyoutlook.org/media/weowebsite/2013/weo2013_ch06_renewables.pdf.]

İzgi, E., A. Öztopal, B. Yerli, M. K. Kaymak, and A. D. Şahin, 2012: Short–mid-term solar power prediction by using artificial neural networks. *Sol. Energy*, **86**, 725–733, doi:10.1016/j.solener.2011.11.013.

Jamaly, M., J. L. Bosch, and J. Kleissl, 2013: Aggregate ramp rates of distributed photovoltaic systems in San Diego County. *IEEE Trans. Sustainable Energy*, **4**, 519–526, doi:10.1109/TSTE.2012.2201966.

Jewell, W. T., and T. D. Unruh, 1990: Limits on cloud-induced fluctation in photovoltaic generation. *IEEE Trans. Energy Convers.*, **5**, 8–14, doi:10.1109/60.50805.

Kleissl, J., 2013: Final project report: Improving economics of solar power through resource analysis, forecasting, and dynamic

system modeling. California Public Utilities Commission Tech. Rep., 71 pp.

——, M. Lave, M. Jamaly, and J. L. Bosch, 2012: Aggregate solar variability. *Power and Energy Society General Meeting*, San Diego, CA, IEEE, doi:10.1109/PESGM.2012.6344809.

Kuleshov, Y., G. de Hoedt, W. Wright, and A. Brewster, 2002: Thunderstorm distribution and frequency in Australia. *Aust. Meteor. Mag.*, **51**, 145–154 pp.

Lave, M., and J. Kleissl, 2010: Solar variability of four sites across the state of Colorado. *Renew. Energy*, **35**, 2867–2873, doi:10.1016/j.renene.2010.05.013.

——, and ——, 2013: Cloud speed impact on solar variability scaling – Application to the wavelet variability model. *Sol. Energy*, **91**, 11–21, doi:10.1016/j.solener.2013.01.023.

——, ——, and E. Arias-Castro, 2012: High-frequency irradiance fluctuations and geographic smoothing. *Sol. Energy*, **86**, 2190–2199, doi:10.1016/j.solener.2011.06.031.

Lorenz, E., and Coauthors, 2009: Benchmarking of different approaches to forecast solar irradiance. *Proc. 24th European Photovoltaic Solar Energy Conf.*, Hamburg, Germany, EU PVSEC, 4199–4208.

Maisano, J., A. Radchik, and I. Skryabin, 2016: A method of forecasting wholesale electricity market prices. *J. Energy Markets*, **9**, 1, 22 pp. [Available online at http://www.risk.net/journal-of-energy-markets/technical-paper/2442390/a-method-of-forecasting-wholesale-electricity-market-prices.]

Marquez, R., H. T. Pedro, and C. F. Coimbra, 2013: Hybrid solar forecasting method uses satellite imaging and ground telemetry as inputs to ANNs. *Sol. Energy*, **92**, 176–188, doi:10.1016/j.solener.2013.02.023.

Mathiesen, P., J. M. Brown, and J. Kleissl, 2013: Geostrophic wind dependent probabilistic irradiance forecasts for coastal California. *IEEE Trans. on Sustainable Energy*, **4**, 510–518, doi:10.1109/TSTE.2012.2200704.

Meyer, M. B., and G. G. Lala, 1990: Climatological aspects of radiation fog occurrence at Albany, New York. *J. Climate*, **3**, 577–586, doi:10.1175/1520-0442(1990)003<0577:CAORFO>2.0.CO;2.

Murata, A., H. Yamaguchi, and K. Otani, 2009: A method of estimating the output fluctuation of many photovoltaic power generation systems dispersed in a wide area. *Electr. Eng. Japan*, **166**, 9–19, doi:10.1002/eej.20723.

Nonnenmacher, L., A. Kaur, and C. F. Coimbra, 2014: Verification of the SUNY direct normal irradiance model with ground measurements. *Sol. Energy*, **99**, 246–258, doi:10.1016/j.solener.2013.11.010.

Physick, W. L., 1988: Mesoscale modeling of a cold front and its interaction with a diurnally heated land mass. *J. Atmos. Sci.*, **45**, 3169–3187, doi:10.1175/1520-0469(1988)045<3169:MMOACF>2.0.CO;2.

Reikard, G., 2009: Predicting solar radiation at high resolutions: A comparison of time series forecasts. *Sol. Energy*, **83**, 342–349, doi:10.1016/j.solener.2008.08.007.

Shi, J., W.-J. Lee, Y. Liu, and Y. Yang, 2011: Forecasting power output of photovoltaic system based on weather classification and support vector machine. *Proc. Industry Applications Society Annual Meeting (IAS)*, Orlando, FL, IEEE, doi:10.1109/IAS.2011.6074294.

Speer, M., and B. Geerts, 1994: A synoptic-mesoalpha-scale climatology of flash-floods in the Sydney metropolitan area. *Aust. Meteor. Mag.*, **43**, 87–103.

Sturman, A., and N. Tapper, 2005: *The Weather and Climate of Australia and New Zealand*. 2nd ed. Oxford University Press, 541 pp.

SunWiz, 2012: Solar PV forecast for AEMO 2012-2022. SunWiz Tech. Rep., SunWiz Consulting and Solar Business Services, Byron Bay, NSW, Australia, 49 pp.

Tapp, R., and S. Barrell, 1984: The north-west Australian cloud band: Climatology, characteristics and factors associated with development. *Int. J. Climatol.*, **4**, 411–424, doi:10.1002/joc.3370040406.

Wong, K., C. Yip, and P. Li, 2008: Automatic identification of weather systems from numerical weather prediction data using genetic algorithm. *Expert Syst. Appl.*, **35**, 542–555, doi:10.1016/j.eswa.2007.07.032.

Yang, H. T., C. M. Huang, Y. C. Huang, and Y. S. Pai, 2014: A weather-based hybrid method for 1-day ahead hourly forecasting of PV power output. *IEEE Trans. Sustainable Energy*, **5**, 917–926, doi:10.1109/TSTE.2014.2313600.

Zehner, M., and Coauthors, 2010: Systematic analysis of meteorological irradiation effects. *Proc. 25th European Photovoltaic Solar Energy Conf.*, Hamburg, Germany, Joint Research Centre, 4545–4548.